Atmos. Chem. Phys. Discuss., 12, 13553–13580, 2012
www.atmos-chem-phys-discuss.net/12/13553/2012/
doi:10.5194/acpd-12-13553-2012


Atmospheric Chemistry and Physics Discussions



# Occurrence of lower cloud albedo in ship tracks

**Y.-C. Chen[1], M. W. Christensen[2], L. Xue[3], A. Sorooshian[4], G. L. Stephens[5], R. M. Rasmussen[3], and J. H. Seinfeld[1,6]**

[1]Division of Engineering and Applied Science, California Institute of Technology, Pasadena, California, USA
[2]Department of Atmospheric Science, Colorado State University, Fort Collins, Colorado, USA
[3]National Center for Atmospheric Research (NCAR), Boulder, Colorado, USA
[4]Department of Chemical and Environmental Engineering/Atmospheric Sciences, The University of Arizona, Arizona, USA
[5]Jet Propulsion Laboratory, California Institute of Technology, Pasadena, California, USA
[6]Division of Chemistry and Chemical Engineering, California Institute of Technology, Pasadena, California, USA

Received: 9 May 2012 – Accepted: 10 May 2012 – Published: 31 May 2012

Correspondence to: J. H. Seinfeld (seinfeld@caltech.edu)

Published by Copernicus Publications on behalf of the European Geosciences Union.







## Abstract

The concept of geoengineering by marine cloud brightening is based on seeding marine stratocumulus clouds with sub-micrometer sea-salt particles to enhance the cloud droplet number concentration and cloud albedo, thereby producing a climate cooling effect. The efficacy of this as a strategy for global cooling rests on the extent to which aerosol-perturbed marine clouds will respond with increased albedo. Ship tracks, cloud regions impacted by ship exhaust, are a well-known manifestation of the effect of aerosol injection on marine clouds. We present here an analysis of the albedo responses in ship tracks, based on in situ aircraft measurements and three years of satellite observations of 589 individual ship tracks. It is found that the sign (increase or decrease) and magnitude of the albedo response in ship tracks depends on the mesoscale cloud structure, the free tropospheric humidity, and cloud top height. In a closed cell structure (cloud cells ringed by a perimeter of clear air), nearly 30 % of ship tracks exhibited a decreased albedo. Detailed cloud responses must be accounted for in global studies of the potential efficacy of sea-spray geoengineering as a means to counteract global warming.

## 1 Introduction

Marine stratocumulus clouds (MSc), covering, on average, nearly one-third of the ocean surface (Warren et al., 1988), exert a cooling influence on climate. It has been estimated that a 6 % increase of the albedo of MSc would offset the warming by atmospheric $CO_2$ doubling (Latham et al., 2008). Based on the assumption that increasing aerosol number concentration leads to higher cloud droplet number concentration and an increase in cloud albedo (Twomey, 1991) (assuming constant liquid water path (LWP)), a marine geo-engineering scheme was proposed (Salter et al., 2008): using wind-driven spray-vessels that pump sub-micrometer sea-salt particles into the air beneath MSc. The effect of injecting aerosols into the marine boundary layer has





ACPD
12, 13553–13580, 2012



been evaluated in several global climate modeling studies with prescribed enhanced cloud droplet number concentration (Jones et al., 2009; Rasch et al., 2009; Bala et al., 2011), global aerosol microphysics models (Korhonen et al., 2010; Partanen et al., 2012; Pringle et al., 2012), parcel models (Russell et al., 1999; Bower et al., 2006), and cloud-system resolving models (Wang et al., 2011).

According to IPCC (2007), the median value of global aerosol indirect radiative forcing is $-0.7\,\mathrm{W\,m^{-2}}$, with an uncertainty range from $-1.8$ to $-0.3\,\mathrm{W\,m^{-2}}$. Modeling the global aerosol indirect effect is challenging, as the representations of aerosol-cloud interactions in climate models are necessarily crude (Lohmann and Feichter, 2005). The premise that clouds and precipitation are strongly sensitive to aerosol perturbations must account for mechanisms that buffer the effects of aerosol perturbations (Stevens and Feingold, 2009). As both aerosol levels and meteorology (i.e., large-scale dynamic and thermodynamic state) govern the state of cloudiness, the intertwining of these two factors complicates the interpretation of aerosol-cloud responses (Stevens and Brenguier, 2009).

Ship tracks serve as a well-known manifestation of marine aerosol-cloud interactions. Whereas ample evidence exists that increased aerosol levels lead to more numerous and smaller cloud droplets, the response of cloud macrophysics (i.e., cloud thickness, LWP) to aerosol perturbations is not as clear-cut. Cloud macrophysical responses to increased aerosol levels can lead to either enhancement or diminution of cloud brightening. One of the challenges in understanding the cloud macrophysical responses lies in untangling the aerosol effects from others such as meteorological conditions. By utilizing both in situ aircraft measurements and A-Train satellite data, we present here an analysis of the factors that control the sign and magnitude of the aerosol indirect effect in ship tracks.





ACPD
12, 13553–13580, 2012



## 2 Data description

### 2.1 In-situ E-PEACE data

The Eastern Pacific Emitted Aerosol Cloud Experiment (E-PEACE) aircraft campaign, carried out in July and August 2011 (30 research flights) over the Eastern Pacific adjacent to the coast of Monterey, California, was designed to provide a well-defined data set on MSc responses to ship emissions (Russell et al., 2012). This area of widespread ship traffic is characterized by layers of persistent stratocumulus clouds. The Center for Interdisciplinary Remotely-Piloted Aircraft Studies (CIRPAS) Twin Otter aircraft was employed, with a full payload of state-of-the-art aerosol and cloud instrumentation (Table 1). Over 30 flights, approximately 45 cargo and tanker ships were probed.

The aerosol number concentration was measured by a condensation particle counter (CPC) and a passive cavity aerosol spectrometer probe (PCASP). Cloud droplet size distributions were measured by the cloud, aerosol, and precipitation spectrometer (CAPS), and cloud droplets are defined as those with radius greater than 1.77 µm and smaller than drizzle droplets. Drizzle drop size distribution was measured using the Cloud-Imaging probe (CIP), and drizzle drops are defined as those with radius greater than $\sim 20\,\mu m$. The cloud base and top are defined with cloud droplet number concentration ($N_d$) threshold $> 10\,cm^{-3}$ and liquid water content (LWC) $> 0.01\,g\,m^{-3}$. LWC is calculated by LWC $= \int \frac{4}{3}\pi\rho_w r^3 n(r)dr$, where $\rho_w$ is density of water, $r$ is droplet radius, and $n(r)$ is the droplet number concentration distribution. And LWP $= \sum(z(i+1) - z(i)) \times \left(\frac{LWC(i+1)+LWC(i)}{2}\right)$, where $z(i)$ is the altitude from cloud base ($i = 1$) to cloud top. The cloud effective radius ($R_e$) is calculated using $R_e = \int r^3 n(r)dr / \int r^2 n(r)dr$.

With the drizzle drop size distribution, the rain rate ($mm\,day^{-1}$) is calculated by Zhao et al. (2011): $R = 24 \times 0.6\pi \times 10^{-3} \int_{D_{min}}^{D_{max}} D^3 v(D) n(D) dD$, where $D$ is the raindrop diameter, and $v(D)$ is the droplet terminal velocity ($m\,s^{-1}$), determined by $v(D) = 3.778 \times D^{0.67}$





ACPD
12, 13553–13580, 2012



(Zhang et al., 2001). The cloud base rain rate is averaged over the lower quarter of the cloud depth.

Using the cloud droplet spectrum, the cloud optical depth, $\tau$, is calculated by

$$\tau = \iint 2\pi r^2 n(r) \mathrm{d}r \mathrm{d}z, \tag{1}$$

where the extinction efficiency at visible wavelength is approximately 2 in the geometric optics limit for typical cloud droplet sizes (Seinfeld and Pandis, 2006).

Under adiabatic condition, a relationship between cloud optical depth and cloud droplet number concentration, $N_\mathrm{d}$, can be expressed as (Brenguier et al., 2000):

$$\tau = \frac{9}{10}\left(\frac{4}{3}\pi\right)^{\frac{1}{3}} I_0^{\frac{2}{3}} (kN_\mathrm{d})^{\frac{1}{3}} H^{\frac{5}{3}}, \tag{2}$$

where $I_0 = C_\mathrm{w}/\rho_\mathrm{w}$, $C_\mathrm{w}$ is the moist adiabatic condensation coefficient, $k$ is a parameter inversely proportional to the droplet distribution breadth, and $H$ is cloud thickness. From the approximate cloud albedo (Lacis and Hansen, 1974), $A = \tau/(\tau + 7.7)$, one obtains $\mathrm{d}A/\mathrm{d}\tau = A(1-A)/\tau$. Together with Eq. (2), the susceptibility of cloud albedo to a perturbation in cloud droplet number concentration can be approximated as:

$$\frac{\mathrm{d}A}{\mathrm{d}N_\mathrm{d}} = \frac{A(1-A)}{3N_\mathrm{d}}\left(1 + \frac{\mathrm{d}\ln k}{\mathrm{d}\ln N_\mathrm{d}} + 5\frac{\mathrm{d}\ln H}{\mathrm{d}\ln N_\mathrm{d}}\right). \tag{3}$$

The first term on the R.H.S. of Eq. (3) represents the so-called Twomey effect, the second term is the dispersion effect (i.e., effect of changes in $N_\mathrm{d}$ on the cloud droplet size distribution), and the third term expresses the sensitivity of cloud thickness to aerosol perturbations. The cloud thickness response, which can be either positive or negative, is determined by the balance between the moistening/cooling of the marine boundary layer resulting from precipitation suppression and drying/warming resulting from enhanced entrainment due to increased turbulence (Ackerman et al., 2004; Wood, 2007).





ACPD
12, 13553–13580, 2012



These three effects represented in Eq. (3) are the major ones affecting the response of cloud optical depth to a perturbation in aerosol number concentration. Specific aerosol chemical composition has a secondary effect (Xue et al., 2012). Equation (3) can be applied to the ship exhaust observations, expressing the change between the unperturbed clouds, subject only to the marine background aerosol, and those perturbed by ship exhaust.

For the dispersion effect, the coefficient $k$ is calculated following Lu and Seinfeld (2006) as a function of relative dispersion ($d$) and skewness ($s$) of the droplet number concentration distribution $n(r)$, $k = \frac{\left(1+d^2\right)^3}{\left(sd^3+1+3d^2\right)^2}$, where $d = \sigma/\bar{r}$, $\bar{r}$ is mean droplet radius, $\sigma$ is the standard deviation of droplet spectrum, given by $\sigma = \left(\frac{1}{N_d}\int(r-\bar{r})^2 n(r)\mathrm{d}r\right)^{\frac{1}{2}}$, and skewness $s$ is defined as $s = \frac{1}{\sigma^3 N_d}\int(r-\bar{r})^2 n(r)\mathrm{d}r$.

During four of the research flights, spiral soundings and/or slanted ascents (Fig. 1) were conducted in areas clearly influenced by the exhaust from large tanker/cargo ships and in adjacent areas relatively free of ship exhaust. This provided an ideal condition to probe the detailed response of cloud properties with respect to ship-emitted particles. Ship exhaust and background marine aerosol below cloud, in cloud, and above cloud were probed. During these four flights the entire boundary layer profile of environmental conditions and aerosol/cloud property profiles was obtained. The perturbed clouds were subject to the same background meteorological conditions as those outside the region of exhaust impact. In this study, we focus on these four research flights during E-PEACE.

### 2.2 Satellite: A-Train

Using 1-km MODIS imagery over regions on the globe where MSc are prevalent (i.e., the North Pacific Ocean, and adjacent to the coasts of South America and South Africa), ship tracks were meticulously logged by hand during the period June 2006–December 2009 (Christensen and Stephens, 2012). Polluted and nearby unpolluted





ACPD
12, 13553–13580, 2012



clouds identified from MODIS images were co-located to the closest observation from the Cloud-Aerosol Lidar with Orthogonal Polarization (CALIOP) and cloud profiling radar (CPR) on CloudSat. Droplet effective radius and LWP were derived using the 3.7-μm reflectances. Cloud albedo was calculated using BUGSrad (Stephens et al., 2001), a two-stream raidative transfer model. In total, 589 ship tracks were identified. Clouds were classified subjectively as closed cell, open cell, unclassifiable, or others (rolled, wavy, streets, etc.) by visually inspecting the region of clouds in a MODIS image (0.64-μm channel) surrounding the ship track. An automated pixel identification scheme, outlined in Christensen and Stephens (2012), was applied to each ship track domain in order to isolate the 1-km MODIS pixels in the ship track from the surrounding unpolluted clouds. Segments, 30 km in length, containing many pixels were used to construct reasonably representative averages of the cloud optical properties derived from MODIS for the polluted and unpolluted portions of ship track domains.

## 3 Results

### 3.1 Cloud response in ship tracks: in situ observations

During four of the research flights (RF18, 19, 20, and 24) with ideal conditions, the detailed response of cloud properties with respect to ship-emitted particles were probed. In each case, the clouds showed marked differences in the microphysical (e.g., effective radius) and macrophysical properties between the unperturbed clouds (in the absence of ship emissions) and those impacted by ship plumes. The perturbed clouds exhibited higher cloud droplet number concentration, $N_d$, and smaller $R_e$ (Table 2 and Fig. 2), consistent with findings in past field studies of ship tracks (e.g., Radke et al., 1989; Hudson and Yum, 1997; Durkee et al., 2000; Brenguier et al., 2000; Twohy et al., 2005; Lu et al., 2007).

During RF20 (4 August 2011), the clouds were heavily drizzling (Table 2). The presence of heavy drizzle produced an open-cell-like cloud structure (i.e., open spaces





ACPD
12, 13553–13580, 2012



ringed by cloud edges, Fig. 3a). Previous studies (Stevens et al., 2005; vanZanten et al., 2005; Savic-Jovcic and Stevens, 2008; Wang and Feingold, 2009) have shown that appreciable precipitation can lead to patchy, scattered cloud, associated with open cellular structures. In the presence of heavy drizzle and solar heating, drizzle evaporation below cloud base and solar absorption tend to promote a stable density stratification within the marine boundary layer (e.g., Stevens et al., 1998; Lewellen and Lewellen, 2002). In the cloud region impacted by the injection of ship exhaust, significant increases in cloud thickness (Clean = 252 m, Ship = 344 m) and LWP (Clean = 41.5 g m$^{-2}$, Ship = 158.5 g m$^{-2}$) were observed, and the cloud albedo is estimated to have increased by 83 % (using Eq. 2; Table 3). For this optically thin cloud with an open cell structure and low background aerosol number concentration, $N_a$, the injection of ship exhaust produced a much brighter cloud than those neighboring owing to more numerous smaller droplets and higher LWP. Also, numerous smaller droplets in ship tracks resulted in less efficient coalescence and a slightly lower cloud base precipitation rate, corroborating the argument in Albrecht (1989). This response has been observed in previous field studies (e.g., Ferek et al., 1998; Lu et al., 2007).

During RF18, 19, and 24, an overcast sky existed with closed cell cloud structures (Fig. 3b). The clouds were non-drizzling in RF18, and lightly drizzling in RF19 and 24. A reduced cloud base rain rate was also evident in RF19 and RF24 ship exhaust-perturbed conditions. Reduced sedimentation of cloud droplets near the cloud top entrainment zone tends to cause more efficient cloud top evaporation, enhancing turbulent kinetic energy and entrainment, and leading to smaller LWP and a thinner cloud (Bretherton et al., 2007). These phenomena (less precipitation, higher vertical velocity variance, lower LWP and thinner cloud) are evident in RF18 and 24 (Table 2).

Among the three closed cell cases, the perturbed cloud in RF19 had higher LWP, cloud thickness, and optical depth than the adjacent clean cloud, similar to that observed in the open cell cloud in RF20. However, the opposite response was observed in RF18 and 24, where decreases in LWP, cloud thickness, and optical depth in the ship track region were found. The difference in cloud macrophysical responses among





ACPD
12, 13553–13580, 2012



these cases can be explained by the ambient thermodynamic conditions. The dewpoint depression (i.e., difference between temperature and dewpoint temperature, an estimate of moisture) above cloud top was much larger in RF18 and 24 as compared to RF19 and 20, indicating a drier free troposphere in these two cases (Table 3). The temperature and humidity variations near cloud top reflect the processes of cloud top entrainment warming and drying (positive $d\theta/dz$ and negative $dq/dz$ near cloud top; not shown). As the boundary layer dried, the cloud base increased and cloud top height decreased, leading to a thinner cloud. Entrainment drying dominated the response of cloud water (Ackerman et al., 2004). Also, the lower tropospheric stability (LTS) was larger in these two cases as compared to RF19 and 20 (Table 3). Higher stability indicated less boundary layer mixing, and led to a diminished moisture supply from the ocean surface, and thus a drier boundary layer. In RF18 and RF24, with drier air above the cloud deck and a relatively stable atmosphere in the closed cell cloud structure, not only did the LWP decrease, but the cloud optical depth also decreased by 20.7 % and 7.8 %, respectively.

The susceptibility of cloud albedo to increased $N_d$ (i.e., $dA/dN_d$), as expressed in Eq. (3), was calculated for these four cases to evaluate the change between the unperturbed clouds and those perturbed by ship emission. The negative albedo response (i.e., lower albedo with increased $N_d$) observed in RF18 and RF24 is consistent with Eq. (3). In both cases, the cloud thickness effect is negative (Fig. 4), as stronger entrainment drying/warming and a stable atmosphere led to a thinner cloud. The dispersion effect is also slightly negative in these two cases, that is, the droplet size spectrum broadens with increased aerosol concentration. The broadening of the spectrum is caused by the competition for water vapor in the relatively polluted, condensation-dominated regime (Feingold and Seibert, 2009). Though the Twomey effect is always positive, it is offset by the negative cloud thickness effect, as the cloud optical depth is five times more sensitive to changes in cloud thickness (Eq. 3). Combined, these effects produced 11.8 % and 2.2 % (for RF18 and RF24, respectively) decreases in cloud albedo in the ship track region.





ACPD
12, 13553–13580, 2012



In RF20, with an open cell cloud structure and an optically thin cloud, the cloud susceptibility is the largest among the four cases. The Twomey effect, dispersion effect, and cloud thickness effect are all positive, with the largest contribution coming from the cloud thickness effect (Fig. 4). The dispersion effect is positive, as the droplet size spectrum narrows. In RF19, with a closed cell cloud structure, cloud susceptibility is also positive. In these two cases (RF19 and RF20), the relatively moist overlying air led to less efficient entrainment drying, resulting in higher LWP and albedo (cloud brightening).

### 3.2 Cloud response in ship tracks: A-Train observations

Using 1-km MODIS imagery during the period June 2006–December 2009, 589 ship tracks were classified as closed cell, open cell, unclassifiable, or others by visually inspecting the cloud regions surrounding each ship track using MODIS images.

Among the 589 ship tracks identified, ship plumes enhanced the cloud albedo ~ 75 % of the time, while ~ 25 % of the time, a decrease in cloud albedo was observed. Ship tracks were separated into two categories: those with enhanced albedo (cloud brightening) and those with diminished albedo (cloud dimming) as compared to the surrounding clouds (Fig. 5). The average dewpoint depression (average moisture profile above the boundary layer from ECMWF-AUX reanalysis data) is higher in cloud dimming cases (24.0 K) than those in cloud brightening cases (18.0 K), consistent with the findings from the in-situ E-PEACE data. Also, the average cloud top height is higher in cases of reduced albedo, as a higher cloud top suggests a greater chance for the cloud layer to be decoupled from the surface moisture supply. Higher clouds, which are relatively decoupled and consequently not as susceptible to aerosol perturbations, were found to exhibit more frequent reduced cloud albedo than lower clouds. A dependence of albedo response on cloud top height was not observed during the E-PEACE in situ flights as the cloud top heights were all below 650 m. Based on the satellite data, the impacts of effective radius and optical depth on albedo response are less evident (Fig. 5). Generally, the average effective radius is slightly smaller, and the average





ACPD
12, 13553–13580, 2012



optical depth is slightly higher in ship tracks for which a dimming response was observed than those with brightening response. In Christensen and Stephens (2012), the optically thin clouds with larger droplets were the most susceptible to a cloud albedo increase. Based on satellite data, the effect of LTS (here defined as the difference in potential temperature at 700 mb and that at surface) on cloud albedo response is muted, as the average LTS is 22.2 (3.5) and 22.2 (3.3) K for the cloud brightening and dimming regimes, respectively (standard deviation in parenthesis; figure not shown).

The relative change of cloud thickness (or LWP) versus the Twomey effect determines, in short, the cloud albedo response. The dispersion effect is of secondary significance (Fig. 4; also in Chen et al., 2011). Based on Eq. (3), assuming the cloud thickness effect remains constant under quasi-instantaneous changes (i.e., the timescale over which the cloud microphysics adjusts to changes in aerosol concentration is rapid (order of minutes) compared to the macrophysical adjustment timescale), the cloud susceptibility is simply the Twomey effect, and can be expressed as:

$$\frac{\Delta A}{A(1-A)} = \frac{1}{3}\Delta(\ln N_{\mathrm{d}}). \quad (4)$$

When the perturbed and unperturbed clouds are macrophysically similar (i.e., red dots in Fig. 6, defined by the absolute value of the fractional change in LWP and cloud top height less than 5 %), the regime is defined as the Twomey regime ($\sim$ 30 % of ship tracks). As expected, at nearly constant LWP, cloud albedo is higher in the perturbed clouds compared to the surroundings, primarily resulting from increased $N_{\mathrm{d}}$. When the macrophysical differences between perturbed and unperturbed clouds are larger (black dots in Fig. 6, in which clouds interact with the environment, leading to change in LWP), the differences in LWP govern the magnitude and sign of the cloud albedo response. With increased LWP in the ship track, the cloud albedo is influenced beyond that predicted by the Twomey effect and, in some ship tracks, the loss in LWP was so great that the cloud albedo enhancement was dimished to the point where complete cancellation occurred. The four in situ E-PEACE data points (Fig. 6) lie generally within the range of the satellite data distribution.





ACPD
12, 13553–13580, 2012



As the albedo response of the clouds is, to some extent, linked to the cloud top altitude and the dryness of the air above, the effects of the cloud top height and dew point depression on the fractional change in cloud albedo, $R_e$, LWP, and $H$ can be seen (Fig. 7). The impact of the ship plumes on cloud droplet effective radius is relatively constant with cloud top height. On the other hand, fractional changes in LWP caused by the plume become increasingly negative as the cloud top height increases, in agreement with Christensen and Stephens (2012). Also, as the dew point depression above cloud top increases (drier air), the fractional change in LWP becomes increasingly negative. As the cloud albedo response follows closely the LWP response, the cloud brightening diminishes as the cloud top altitudes decrease and the free troposphere becomes drier. Cloud top height and dewpoint depression exert strong controls on the LWP response.

In the closed cell regime, nearly 30 % of ship tracks exhibit decreased cloud albedo. In the open cell and unclassifiable regimes, ∼ 14 % and 19 % of the ship tracks, respectively, also exhibit decreased albedo.

## 4 Conclusions

The coupling among aerosol, cloud, precipitation, and meteorological conditions in the marine boundary layer is complex (Fig. 8). In this study, we evaluate, based on both in-situ and satellite data, the effect of environmental conditions, cloud cellular structures, and cloud properties (e.g., cloud top height, extent of drizzle) on cloud albedo responses to ship emissions. Cloud brightening is evident in an open cellular cloud structure, and with relatively moist air above cloud tops. The opposite effect appears in the presence of a drier free troposphere and stable atmosphere in a closed cellular cloud structure. With sufficiently dry air above cloud tops, the enhanced entrainment drying/warming facilitated by smaller droplets in polluted clouds leads to lower LWP and thinner clouds. Also, increased stability led to less efficient boundary layer mixing and decreased moisture supply from the ocean. When the negative cloud thickness effect outweighs the positive Twomey effect (Eq. 3), a lower cloud albedo results. Based





ACPD
12, 13553–13580, 2012



on over 3 yr of satellite data, both the dryness of the air above marine boundary layer and cloud top heights are seen to play significant roles in determining the albedo response. In the cases in which cloud albedo actually decreased, cloud top heights were deeper and capped by very dry overlying air. In classification of cloud cellular regimes, 30 % of the closed cell ship tracks exhibited lower cloud albedo.

Cloud macrophysical responses are crucial in determining both the strength and the sign of the cloud albedo response to aerosols intentionally injected into the marine boundary layer. These responses must be accounted for in global studies of the potential efficacy of sea spray geo-engineering as a means to counteract global warming.

*Acknowledgements.* This work was supported by Office of Naval Research grants N00014-10-1-0200 and N00014-10-1-0811, and National Science Foundation grant AGS-1008848. Y.-C. C. thanks D. Axisa, Z. Wang and H. Duong for help on aircraft data analysis.

## References

Ackerman, A. S., Kirkpatrick, M. P., Stevens, D. E., and Toon, O. B.: The impact of humidity above stratiform clouds on indirect aerosol climate forcing, Nature, 432, 1014–1017, 2004. 13557, 13561, 13580

Albrecht, B.: Aerosols, cloud microphysics, and fractional cloudiness, Science, 245, 1227–1230, doi:10.1126/science.245.4923.1227, 1989. 13560, 13580

Bala, G., Caldeira, K., Nemani, R., Cao, L., Ban-Weiss, G., and Shin, H.-J.: Albedo enhancement of marine cloud to counteract global warming: impacts on the hydrological cycle, Clim. Dynam., 37, 915–931, doi:10.1007/s00382-010-0868-1, 2011. 13555

Bower, K., Choularton, T., Latham, J., Sahraei, J., and Salter, S.: Computational assessment of a proposed technique for global warming mitigation via albedo-enhancement of marine stratocumulus clouds, Atmos. Res., 82, 328–336, doi:10.1016/j.atmosres.2005.11.013, 2006. 13555

Brenguier, J.-L., Pawloska, H., Schüller, L., Preusker, R., and Fischer, J.: Radiative propertiesof boundary layer clouds: Droplet effective radius versus number concentration, J. Atmos. Sci., 57, 803–821, 2000. 13557, 13559





ACPD

12, 13553–13580, 2012



Bretherton, C. S., Blossey, P. N., and Uchida, J.: Cloud droplet sedimentation, entrainment efficiency, and subtropical stratocumulus albedo, Geophys. Res. Lett., 34, L03813, doi:10.1029/2006GL027648, 2007. 13560, 13580

Chen, Y.-C., Xue, L., Lebo, Z. J., Wang, H., Rasmussen, R. M., and Seinfeld, J. H.: A comprehensive numerical study of aerosol-cloud-precipitation interactions in marine stratocumulus, Atmos. Chem. Phys., 11, 9749—9769, doi:10.5194/acp-11-9749-2011, 2011. 13580

Christensen, M. W. and Stephens, G. L.: Microphysical and macrophysical responses of marine stratocumulus polluted by underlying ships. Part 2: Impacts of haze on precipitating clouds, J. Geophys. Res., doi:10.1029/2011JD017125, in press, 2012. 13558, 13559, 13563, 13564

Durkee, P. A., Noone, K. J., and Bluth, R. T.: The Monterey area ship track experiment, J. Atmos. Sci., 57, 2523–2541, doi:10.1175/1520-0469(2000)057⟨2523:TMASTE⟩2.0.CO;2, 2000. 7 13559

Feingold, G. and Seibert, H.: Cloud-Aerosol Interactions from the micro to cloud scale, in: Clouds in the perturbed climate system: their relationship to energy balance, atmospheric dynamics, and precipitation, edited by: Heintzenberg, J. and Charlson, R. J., MIT Press, 2009. 13561

Ferek, R. J., Hegg, D. A., Hobbs, P. V., Durkee, P., and Nielsen, K.: Measurements of ship-induced cloud tracks off the Washington coast, J. Geophys. Res., 103, 23 199–23 206, doi:10.1029/98JD02121, 1998. 13560

Hudson, J. G. and Yum, S. S.: Droplet spectral broadening in marine stratus, J. Atmos. Sci., 54, 2642–2654, doi:10.1175/1520-0469(1997)054⟨2642:DSBIMS⟩2.0.CO;2, 1997. 13559

IPCC: Summary for Policymakers, in: Climate Change 2007: The Physical Science Basis. Contribution of Working Group I to the Fourth Assessment Report of the Intergovernmental Panel on Climate Change, edited by: Solomon, S., Qin, D., Manning, M., Chen, Z., Marquis, M., Averyt, K. B., Tignor, M., and Miller, H. L., Cambridge University Press, 2007. 13555

Jones, A., Haywood, J., and Boucher, O.: Climate impacts of geoengineering marine stratocumulus clouds, J. Geophys. Res., 114, D10106, doi:10.1029/2008JD011450, 2009. 13555

Korhonen, H., Carslaw, K. S., and Romakkaniemi, S.: Enhancement of marine cloud albedo via controlled sea spray injections: a global model study of the influence of emission rates, microphysics and transport, Atmos. Chem. Phys., 10, 4133–4143, doi:10.5194/acp-10-4133-2010, 2010. 13555





ACPD
12, 13553–13580, 2012



Lacis, A. A. and Hansen, J. E.: A parameterization for the absorption of solar radiation in the Earth's atmosphere, J. Atmos. Sci., 31, 118–133, doi:dx.doi.org/10.1175/1520-0469(1974)031⟨0118:APFTAO⟩2.0.CO;2, 1974. 13557

Latham, J., Rasch, P., Chen, C.-C., Kettles, L., Gadian, A., Gettelman, A., Morrison, H., Bower, K., and Choularton, T.: Global temperature stabilization via controlled albedo enhancement of low-level maritime clouds, Philos. Trans. Roy. Soc. London, 366, 3969–3987, doi:10.1098/rsta.2008.0137, 2008. 13554

Lewellen, D. C. and Lewellen, W. S.: Entrainment and decoupling relations for cloudy boundary layers, J. Atmos. Sci., 59, 2966–2986, doi:10.1175/1520-0469(2002)059⟨2966:EADRFC⟩2.0.CO;2, 2002. 13560

Lohmann, U. and Feichter, J.: Global indirect aerosol effects: a review, Atmos. Chem. Phys., 5, 715–737, doi:10.5194/acp-5-715-2005, 2005. 13555

Lu, M. and Seinfeld, J. H.: Effect of aerosol number concentration on cloud droplet dispersion: A large-eddy simulation study and implications for aerosol indirect forcing, J. Geophys. Res., 111, doi:10.1029/2005JD006419, 2006. 13558

Lu, M.-L., Conant, W. C., Jonsson, H. H., Varutbangkul, V., Flagan, R. C., and Seinfeld, J. H.: The Marine Stratus/Stratocumulus Experiment (MASE): Aerosol-cloud relationships in marine stratocumulus, J. Geophys. Res., 112, D10209, doi:10.1029/2006JD007985, 2007. 13559, 13560

Partanen, A.-I., Kokkola, H., Romakkaniemi, S., Kerminen, V.-M., Lehtinen, K. E. J., Bergman, T., Arola, A., and Korhonen, H.: Direct and indirect effects of sea spray geoengineering and the role of injected particle size, J. Geophys. Res., 117, D02203, doi:10.1029/2011JD016428, 2012. 13555

Pringle, K. J., Carslaw, K. S., Fan, T., Mann, G., Hill, A., Stier, P., Zhang, K., and Tost, H.: A multi-model assessment of theefficacy of sea spray geoengineering, Atmos. Chem. Phys. Discuss, 12, 7125–7166, doi:10.5194/acpd-12-7125-2012, 2012. 13555

Radke, L. F., Coakley, J. A., and King, M. D.: Direct and remote sensing observations of the effects of ships on clouds, Science, 246, 1146–1149, doi:10.1126/science.246.4934.1146, 1989. 13559

Rasch, P. J., Latham, J., and Chen, C.-C.: Geoengineering by cloud seeding: influence on sea ice and climate system, Environ. Res. Lett., 4, 1290–1301, doi:10.1088/1748-9326/4/4/045112, 2009. 13555





ACPD
12, 13553–13580, 2012



Russell, L. M., Seinfeld, J. H., Flagan, R. C., Ferek, R. J., Hegg, D. A., Hobbs, P. V., Wobrock, W., Flossmann, A., O'Dowd, C. D., Nielsen, K. E., and Durkee, P. A.: Aerosol dynamics in ship tracks, J. Geophys. Res., 104, 31 077–31 095, 1999. 13555

Russell, L. M., Sorooshian, A., Seinfeld, J. H., Albrecht, B. A., Nenes, A., Ahlm, L., Chen, Y.-C., Coggon, M., Craven, J. S., C., F. R., Frossard, A. A., H., J., Jung, E., Lin, J. J., Metcalf, A. R., Modini, R., Muelmenstaedt, J., Roberts, G. C., Shingler, T., Song, S., Wang, Z., and Wonaschuetz, A.: Eastern Pacific Emitted Aerosol Cloud Experiment (E-PEACE), Bull. Amer. Meteorol. Soc., submitted, 2012. 13556

Salter, S., Sortino, G., and Latham, J.: Sea-going hardware for the cloud albedo method of reversing global warming, Philos. Trans. Roy. Soc. London, 366, 3989–4006, doi:10.1098/rsta.2008.0136, 2008. 13554

Savic-Jovcic, V. and Stevens, B.: The structure and mesoscale organization of precipitating stratocumulus, J. Atmos. Sci., 65, 1587–1605, 2008. 13560

Seinfeld, J. H. and Pandis, S. N.: Atmospheric Chemistry and Physics, John Wiley and Sons, Inc., Hoboken, NJ, 2 edn., 2006. 13557

Stephens, G. L., Gabriel, P. M., and Partain, P. T.: Parameterization of atmospheric radiative transfer. Part I: Validity of simple models, J. Atmos. Sci., 58, 3391–3409, 2001. 13559

Stevens, B. and Brenguier, J.-L.: Cloud controlling factors: low clouds, in: Clouds in the perturbed climate system: their relationship to energy balance, atmospheric dynamics, and precipitation, edited by: Heintzenberg, J. and Charlson, R. J., 173–196, MIT Press, 2009. 13555

Stevens, B. and Feingold, G.: Untangling aerosol effects on clouds and precipitation in a buffered system, Nature, 461, 607–613, doi:10.1038/nature08281, 2009. 13555

Stevens, B., Cotton, W. R., Feingold, G., and Moeng, C.-H.: Large-eddy simulations of strongly precipitating, shallow, stratocumulus-topped boundary layers, J. Atmos. Sci., 55, 3616–3638, 1998. 13560

Stevens, B., Vali, G., Comstock, K., vanZanten, M. C., Austin, P. H., Bretherton, C. S., and Lenschow, D. H.: Pockets of open cells and drizzle in marine stratocumulus, B. Am. Meteorol. Soc., 86, 51–57, 2005. 13560

Twohy, C. H., Petters, M. D., Snider, J. R., Stevens, B., Tahnk, W., Wetzel, M., Russell, L., and Burnet, F.: Evaluation of the aerosol indirect effect in marine stratocumulus clouds: Droplet number, size, liquid water path, and radiative impact, J. Geophys. Res., 110, D08203, doi:10.1029/2004JD005116, 2005. 13559





ACPD
12, 13553–13580, 2012



Twomey, S.: Aerosols, clouds, and radiation, Atmos. Environ., 25, 2435–2442, 1991. 13554, 13580

vanZanten, M. C., Stevens, B., Vali, G., and Lenschow, D. H.: Observations of Drizzle in Nocturnal marine stratocumulus, J. Atmos. Sci., 62, 88–106, 2005. 13560

Wang, H. and Feingold, G.: Modeling mesoscale cellular structures and drizzle in marine stratocumulus. Part I: Impact of drizzle on the formation and evolution of open cells, J. Atmos. Sci., 66, 3237–3256, 2009. 13560

Wang, H., Rasch, P. J., and Feingold, G.: Manipulating marine stratocumulus cloud amount and albedo: a process-modelling study of aerosol-cloud-precipitation interactions in response to injection of cloud condensation nuclei, Atmos. Chem. Phys., 11, 4237–4249, doi:10.5194/acp-11-4237-2011, 2011. 13555

Warren, S. G., Hahn, C. J., London, J., Chervine, R. M., and Jenne, R. L.: Global distribution of total cloud cover and cloud type amounts over the ocean, NCAR/TN-317 STR, NCAR Tech. Note, 1988. 13554

Wood, R.: Cancellation of aerosol indirect effects in marine stratocumulus through cloud thinning, J. Atmos. Sci., 64, 2657–2669, doi:10.1175/JAS3942.1, 2007. 13557, 13580

Xue, L., Teller, A., Rasmussen, R. M., Geresdi, I., Pan, Z., and Liu, X.: Effects of aerosol solubility and regeneration on mixed-phase orographic clouds and precipitation, J. Atmos. Sci., doi:10.1175/JAS-D-11-098.1, in press, 2012. 13558

Zhang, G., Vivekanandan, J., and Brandes, E.: A method for estimating rain rate and drop size distribution from polarimetric radar measurements, IEEE Trans. Geosci. Remote Sens., 39, 830–841, 2001. 13557

Zhao, G., Chu, R., Zhang, T., Li, J., Shen, J., and Wu, Z.: Improving the rainfall rate estimation in the midstream of the Heihe River Basin using rain drop size distribution, Hydrol. Earth Syst. Sci., 15, 943–951, doi:10.5194/hess-15-943-2011, 2011. 13556





ACPD

12, 13553–13580, 2012



**Table 1.** Instrumentation Payload on CIRPAS Twin Otter.

| Parameter | Instrument | Detected Size |
|---|---|---|
| Particle Number Concentration | Condensation Particle Counter: CPC3010<br>CPC3025 | $D_p^a > 10$ nm<br>$D_p > 3$ nm |
| Aerosol Size Distribution | Passive Cavity Aerosol Spectrometer Probe (PCASP)<br>Scanning Differential Mobility Analyzer (DMA) | 0.1–2.6 µm<br>15 nm–1 µm |
| Cloud and Drizzle Drop Size Distribution | Cloud, Aerosol, and Precipitation Spectrometer[b] (CAPS)<br>Phase Doppler Interferometer (PDI)<br>Forward Scattering Spectrometer Probe (FSSP)<br>Gerber Light Diffraction (PVM-100 probe) | 0.4 µm–1.6 mm<br>4–200 µm<br>1–46 µm<br>~5–50 µm |
| Aerosol Bulk Composition | Aerodyne Time-of-Flight Aerosol Mass Spectrometer (AMS)<br>Single-Particle Soot Photometer (SP2) | $D_{va}^c$ ~40 nm–1 mm |
| Particle Properties | Cloud Condensation Nuclei Counter (CCN Spectrometer)<br>Particle Soot Absorption Photometer (PSAP)<br>Photoacoustic Soot Spectrometer (PASS-3) | |
| Cloud Structures | Frequency-Modulated Continuous-Wave<br>94 GHz Doppler Cloud Radar (upward-facing) | |
| Particle and Droplet Inlets | Counterflow Virtual Impactor (CVI) | |
| Meteorological variables<br>(Temperature, relative humidity, wind properties, etc.) | Meteorology probes | |

[a] Particle diameter.
[b] Drizzle drop size distribution is measured by the Cloud Imaging Spectrometer (CIP-2-D), included in the CAPS package.
[c] Vacuum aerodynamic diameter.





ACPD
12, 13553–13580, 2012



**Table 2.** Aerosol/cloud properties measured during E-PEACE Research Flights 18, 19, 20, and 24. For the cloud structure, closed/open means closed or open cloud cellular structure. Cloud layer is defined with cloud droplet number concentration $> 10\,cm^{-3}$ and liquid water content $> 0.01\,g\,m^{-3}$. Mean $N_a$, $N_d$, $R_e$ (cloud drop effective radius), and $k$ (droplet spectral shape parameter) are geometric mean values. BL average w'w' is the mean vertical velocity variance in the boundary layer. Standard deviation is in parenthesis.

| Research Flight (2011) | | Cloud Structure | Cloud top (m) | Cloud base (m) | Cloud thickness (m) | Mean $N_a$ (> 120 nm) | Mean $N_d$ ($cm^{-3}$) | Mean $R_e$ (μm) | Cloud base rain rate ($mm\,d^{-1}$) | BL mean w'w' ($m^2\,s^{-2}$) | $k$ |
|---|---|---|---|---|---|---|---|---|---|---|---|
| RF18 | Clean | Closed | 609.5 | 460.0 | 149.5 | 153.9 (96.3) | 216.1 (44.1) | 6.15 (0.97) | n/a | 0.214 | 0.81 |
| (2 Aug) | Ship | | 598.8 | 475.3 | 123.5 | 379.5 (137.7) | 316.8 (117.4) | 5.45 (0.84) | n/a | 0.216 | 0.71 |
| RF19 | Clean | Closed | 630.7 | 329.1 | 301.6 | 126.2 (82.4) | 161.4 (33.6) | 8.80 (1.04) | 0.63 (0.28) | 0.239 | 0.74 |
| (3 Aug) | Ship | | 648.2 | 266.2 | 382.0 | 217.6 (111.3) | 341.7 (127.7) | 7.32 (1.18) | 0.60 (0.32) | 0.311 | 0.73 |
| RF20 | Clean | Open | 616.3 | 363.9 | 252.4 | 24.3 (13.8) | 14.0 (6.4) | 16.94 (2.63) | 12.53 (4.03) | 0.103 | 0.39 |
| (4 Aug) | Ship | | 608.6 | 264.8 | 343.8 | 73.4 (43.1) | 39.0 (9.3) | 16.01 (2.73) | 11.40 (3.60) | 0.113 | 0.57 |
| RF24 | Clean | Closed | 607.7 | 238.6 | 369.1 | 115.2 (78.2) | 153.5 (38.7) | 9.27 (1.57) | 1.58 (0.54) | 0.135 | 0.65 |
| (10 Aug) | Ship | | 591.5 | 254.4 | 337.1 | 197.2 (96.0) | 193.5 (80.5) | 8.76 (1.36) | 1.07 (0.59) | 0.200 | 0.63 |





ACPD
12, 13553–13580, 2012



**Table 3.** Cloud LWP, optical properties, and environmental conditions measured during E-PEACE Research Flights 18, 19, 20, and 24. Standard deviation is in parenthesis.

| Research Flight | | LWP ($g m^{-2}$) | Optical depth $\tau$ | Cloud albedo $A$ | $\Delta$LWP/LWP [a] | $\Delta A/A$ | Dewpoint depression [b] (K) | LTS [c] (K) |
|---|---|---|---|---|---|---|---|---|
| RF18 | Clean | 31.0 | 7.3 | 0.49 | −0.33 | −0.12 | 40.0 (1.4) | 15.1 (0.3) |
| (2 Aug.) | Ship | 21.1 | 5.8 | 0.43 | | | | |
| RF19 | Clean | 104.0 | 18.4 | 0.70 | 0.62 | 0.16 | 14.3 (1.4) | 9.7 (0.4) |
| (3 Aug.) | Ship | 168.2 | 35.4 | 0.82 | | | | |
| RF20 | Clean | 41.5 | 4.6 | 0.37 | 2.82 | 0.82 | 2.8 (0.5) | 5.5 (0.3) |
| (4 Aug.) | Ship | 158.5 | 16.4 | 0.68 | | | | |
| RF24 | Clean | 128.6 | 21.8 | 0.74 | −0.17 | −0.02 | 16.9 (1.8) | 13.1 (0.2) |
| (10 Aug.) | Ship | 107.2 | 20.1 | 0.72 | | | | |

[a] Relative LWP difference between exhaust-perturbed and unperturbed clouds.
[b] The free tropospheric dewpoint depression ($T - T_d$) is averaged over the region from 100 m above the cloud top to the highest point reached in the flight (on average 100 to ~ 140 m above cloud top).
[c] Lower tropospheric stability is calculated using $\theta_{925\,mb} - \theta_{sfc}$.





ACPD
12, 13553–13580, 2012



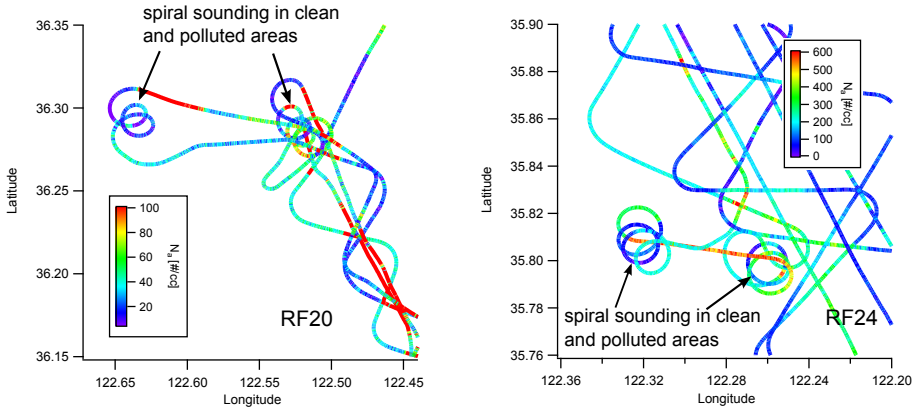


**Fig. 1.** Spiral soundings of clean and ship exhaust perturbed areas in E-PEACE research flight 20 and 24 (4 August and 10 August 2011, respectively). Flight path is colored according to aerosol number concentration (particle diameter > 120 nm).





ACPD
12, 13553–13580, 2012



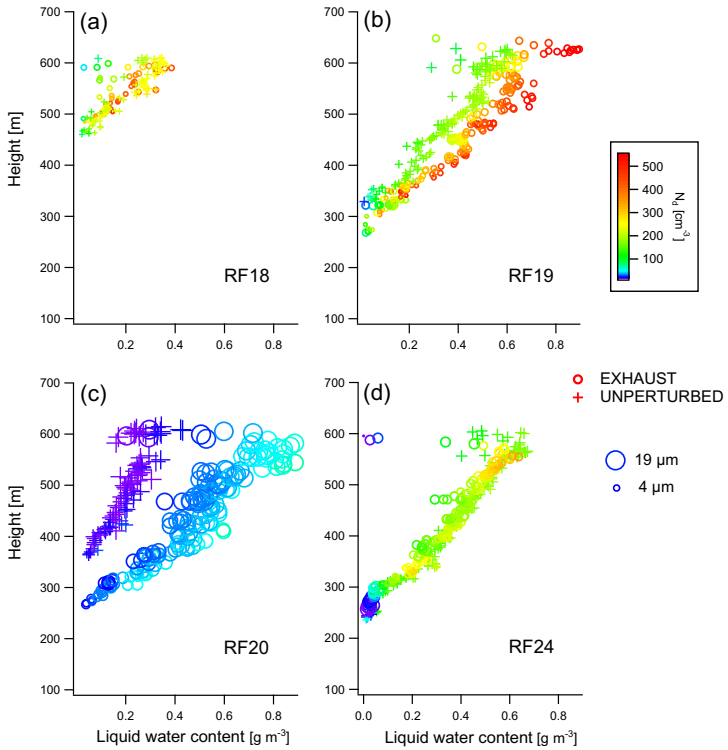


**Fig. 2.** Cloud microphysical parameters measured along the flight tracks. Each symbol represents data over a 1 s increment. Cloud droplet number concentration [$cm^{-3}$] is colored on a logarithmic scale; droplet effective radius is given by the size of symbols varying between ~ 4 and 19 µm. Clean and perturbed cloud data are presented by crosses and open circles, respectively.





ACPD
12, 13553–13580, 2012



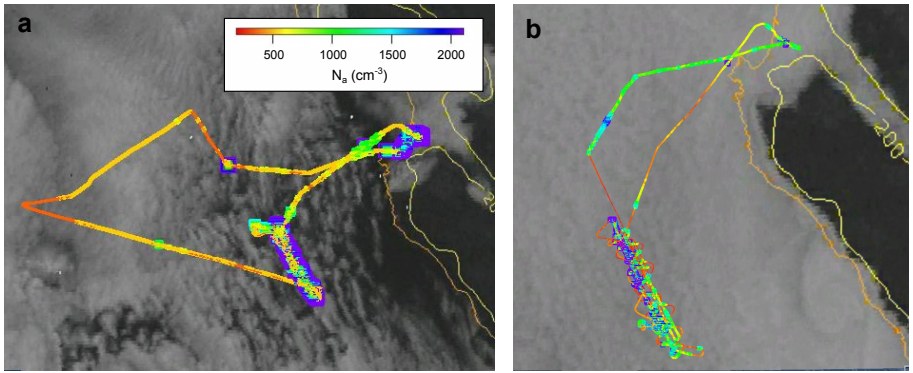


**Fig. 3.** GOES satellite images. Satellite images during **(a)** RF20 (4 August 2011) and **(b)** RF24 (10 August 2011) off coast of Monterey, CA, exemplifying open and closed cell cloud structures, respectively. Flight path is colored according to aerosol number concentration (particle diameter > 10 nm).





ACPD
12, 13553–13580, 2012



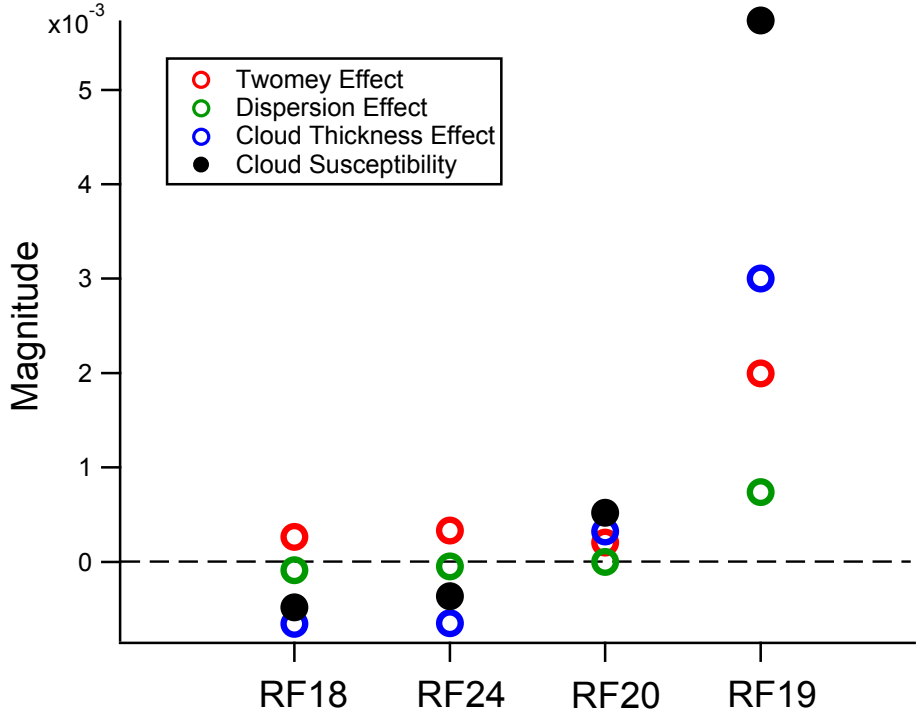


**Fig. 4.** Magnitude of cloud susceptibility in four E-PEACE cases. Twomey effect (red open circle), dispersion effect (green open circle), cloud thickness effect (blue open circle), and total cloud susceptibility (black circle) for RF18, RF24, RF20, and RF19 (order from low to high cloud susceptibility), based on Eq. (3).





ACPD
12, 13553–13580, 2012



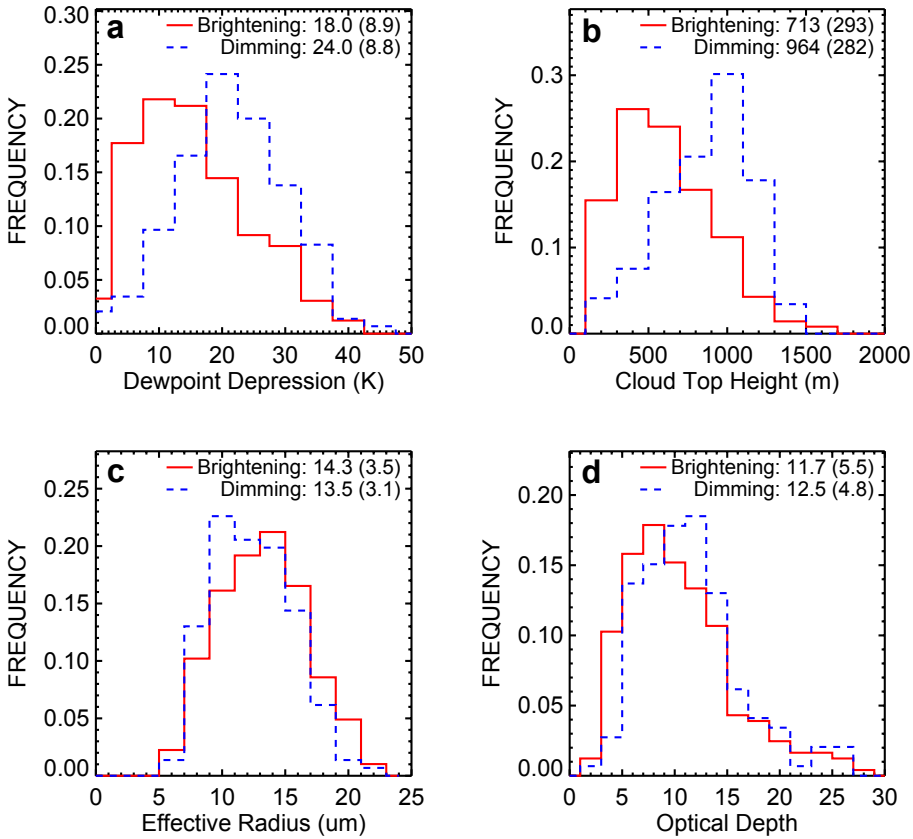


**Fig. 5.** Frequency distribution of different parameters for 589 individual ship tracks from June 2006–December 2009 A-Train observations. The parameters include: **(a)** dew point depression, **(b)** cloud top height, **(c)** effective radius, and **(d)** optical depth. Albedo enhancement (brightening) and decrease (dimming) cases are shown by red and blue lines, respectively. Means and (standard deviations) are given at the top of each panel.





ACPD
12, 13553–13580, 2012



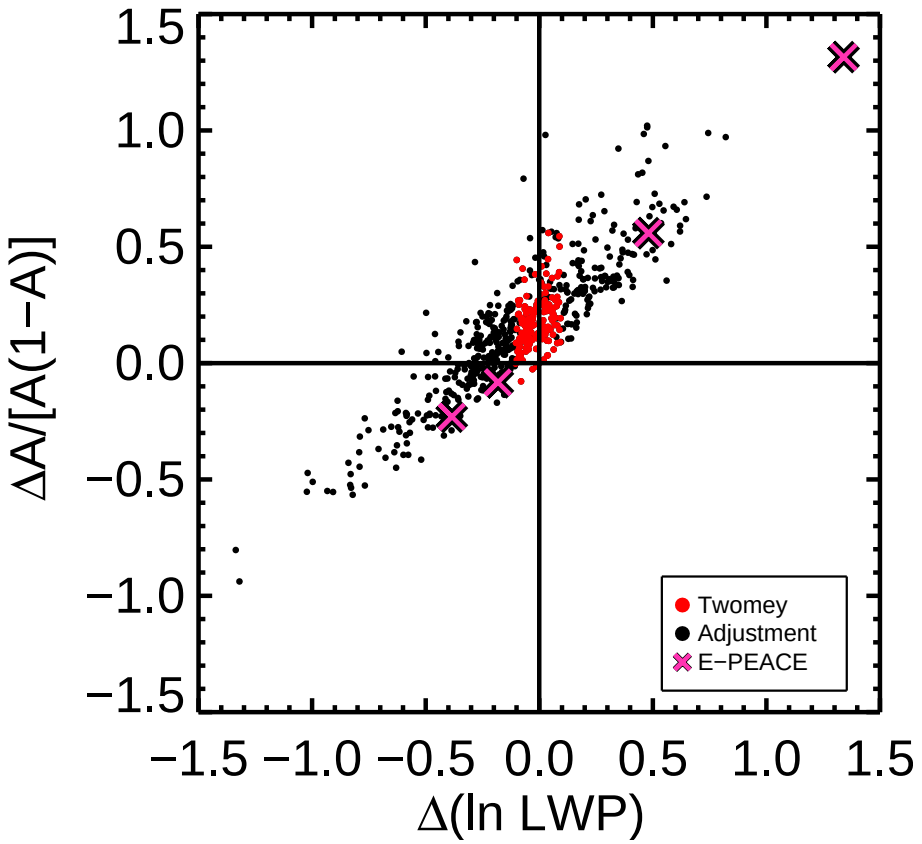


**Fig. 6.** Fractional change in cloud albedo (Eq. 4) versus the fractional change in logarithm LWP. Indicated are the regime of the Twomey effect (red dots, defined by the absolute value of the fractional change in LWP less than 5 %) and of LWP feedback adjustment (black dots, in which clouds interacted with the environment, resulting in change in LWP). The four E-PEACE data points (pink) are shown.





ACPD
12, 13553–13580, 2012



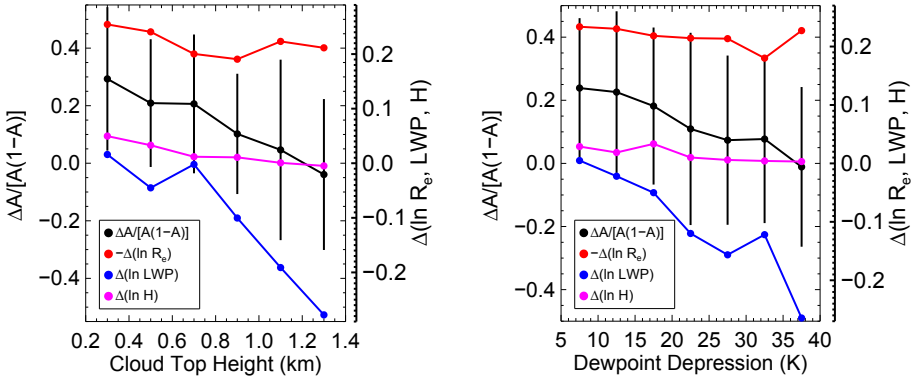


**Fig. 7.** Binned change in albedo, effective radius ($R_e$), LWP, and cloud thickness ($H$) as a function of cloud top height (left panel), and dew point depression (right panel) based on 589 ship tracks observed over June 2006–December 2009. Cases were binned by 200 m in cloud top height and 5 K in dewpoint depression. A minimum of 20 ship tracks was required for each bin.





ACPD
12, 13553–13580, 2012



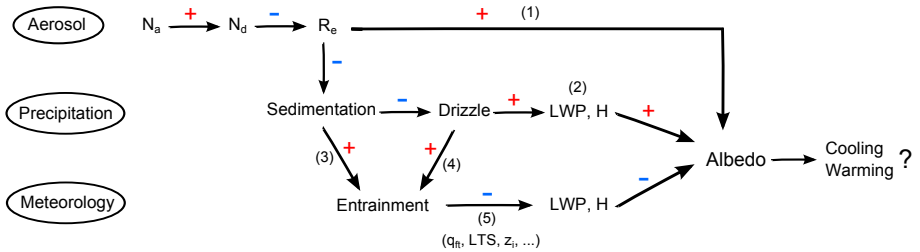


**Fig. 8.** Conceptual diagram displaying the interactions among aerosol, cloud, precipitation, and meteorology. The response of each property/phenomenon to increased aerosol ($N_a$) is shown as a red plus (signifying positive response), and a blue minus (negative response) sign. Footnotes to figure: (1) Twomey effect (Twomey, 1991); assuming LWP is constant. (2) This effect applies in drizzling clouds (Albrecht, 1989). (3) Sedimentation-entrainment effect (Bretherton et al., 2007; Ackerman et al., 2004): reduced in-cloud sedimentation leads to increase of cloud water and evaporation in entrainment regions, resulting in stronger entrainment. (4) Drizzle-entrainment effect (Wood, 2007): less drizzle reduces below-cloud evaporative cooling and in-cloud latent heat release, resulting in higher turbulent kinetic energy and thus stronger entrainment. (5) Significant meteorological conditions, such as free tropospheric humidity ($q_{ft}$), large scale divergence rate, sea surface temperature, can control the MSc structure (Wood, 2007; Chen et al., 2011). The $q_{ft}$, low tropospheric stability (LTS), and cloud top height ($z_i$) may be the key factors controlling the albedo response; cloud top height is determined by large-scale divergence ($D$) and entrainment rate ($E$), following $dz_i/dt = E - Dz_i$.





ACPD
12, 13553–13580, 2012